

# Real-time cosmology with SKA

Yan Liu,<sup>1</sup> Jing-Fei Zhang,<sup>1</sup> and Xin Zhang<sup>\*1,2,3, †</sup>

<sup>1</sup>*Department of Physics, College of Sciences, Northeastern University, Shenyang 110819, China*

<sup>2</sup>*Ministry of Education Key Laboratory of Data Analytics and Optimization for Smart Industry, Northeastern University, Shenyang 110819, China*

<sup>3</sup>*Center for High Energy Physics, Peking University, Beijing 100080, China*

In this work, we investigate what extent the cosmological parameters can be constrained to when the redshift drift data of Square Kilometre Array (SKA) are used alone and what will happen when the European Extremely Large Telescope (E-ELT) and SKA mock data are combined. The  $\Lambda$ CDM model is chosen as a reference model to reach our aims. We find that using the SKA1-only mock data, the  $\Lambda$ CDM model can be loosely constrained, while the model can be well constrained when the SKA2-only mock data are used. When the combination of SKA and E-ELT mock data are considered, the constraints can be significantly improved almost as good as the data combination of the type Ia supernovae observation, the cosmic microwave background observation, and the baryon acoustic oscillations observation. Furthermore, we also investigate in the future what role the redshift drift data of SKA will play in the cosmological parameter estimation. We use four dark energy models, namely, the  $\Lambda$ CDM model, the  $w$ CDM model, the CPL model, and the HDE model, as examples to make the analysis. These models are favored by the current observations well. We find that the redshift drift measurement of SKA could help to significantly improve the constraint on dark energy and could break the degeneracy existing between the cosmological parameters. Therefore, we conclude that redshift-drift observation of SKA would provide a good improvement in the cosmological parameter estimation in the future and have the enormous potential to be one of the most competitive cosmological probes in constraining dark energy.

## I. INTRODUCTION

The accelerated expansion of the universe has been discovered and confirmed by cosmological observations for about twenty years, which is undoubtedly one of the greatest scientific discoveries in the modern cosmology. However, the science behind the cosmic acceleration, i.e., the nature of dark energy, still remains mysterious for us. To measure the physical property of dark energy, one should precisely measure the expansion history of the universe. Currently, the mainstream way is to measure the cosmic distances (luminosity distance or angular diameter distance) and the corresponding redshifts, and to establish a distance-redshift relation, by which constraints on the parameters of dark energy (and other cosmological parameters) can be made. However, a more straightforward way is to directly measure the expansion rate of the universe at different redshifts, although this measurement is more difficult in the observational cosmology.

With the fast advancement in technology over the past several decades, the possibility of measuring the temporal variation of astrophysical observable quantities over a few decades is becoming more and more realistic. This kind of real-time observations can be called the “*real-time cosmology*”. The most typical real time observable is the *redshift drift*, which can give a direct measurement for the expansion rate (namely, the Hubble parameter)

of the universe in a specific range of redshifts.

The approach of measuring the redshift drift was first proposed by Sandage, who suggested a direct measurement of the redshift variation for the extra-galactic sources [1]. At that time, obviously, such a measurement was out of reach with the technological limitation of the day. Then, the method was further improved by Loeb, who suggested a more realistic way of measuring the redshift drift using Lyman- $\alpha$  absorption lines of the distant quasars (QSOs) to detect the redshift variation [2]. Loeb concluded that the signal would be detectable when 100 quasars can be observed over 10 years with a 10-meter class telescope. Thus, the method of redshift drift measurement is also referred to as the “Sandage-Loeb” (SL) test.

Based on the SL test, the scheduled European Extremely Large Telescope (E-ELT), a giant 40-meter class optical telescope, is equipped with a high-resolution spectrograph to perform the COsmic Dynamics EXperiment (CODEX). The experiment is designed to detect the SL-test signals by observing the Lyman- $\alpha$  absorption lines within the redshift range of  $2 \lesssim z \lesssim 5$ . The forecast of using the redshift drift from the E-ELT to constrain dark energy models has been extensively discussed; see, e.g., Refs. [3–13]. It has been shown that the redshift drift in the redshift range of  $2 < z < 5$  is rather useful to break the parameter degeneracies generated by other observations and thus can play an important role in the cosmological estimation in the future.

The Square Kilometre Array (SKA) has recently started construction for the stage of Phase one. Actually, SKA can also perform the research of real-time cosmology. Instead of detecting the Lyman- $\alpha$  absorption lines of

\*Corresponding author

†Electronic address: zhangxin@mail.neu.edu.cn

quasar, SKA will measure the spectral drift in the neutral hydrogen (HI) emission signals of galaxies to implement the measurement of redshift drift in the redshift range of  $0 < z < 1$ . Obviously, the redshift drift data of SKA provide an important supplement to those of E-ELT.

In this work, we will study the real-time cosmology with the redshift drift observation from SKA. We will simulate the redshift drift data of SKA and use these data to constrain cosmological parameters. We have the following aims in this work: (i) We wish to learn what extent the cosmological parameters can be constrained to by using the redshift drift data of SKA-only. (ii) What will happen when the redshift drift data of SKA and E-ELT are combined to perform constraints on cosmological parameters. (iii) What role the redshift drift data of SKA will play in the cosmological estimation in the future.

We will employ several typical and simple dark energy models to perform the analysis of this work. We will consider the  $\Lambda$  cold dark matter ( $\Lambda$ CDM) model in this work, which is the simplest cosmological model and is able to explain the various current cosmological observations quite well. The  $w$ CDM model [14–17] is the simplest extension to the  $\Lambda$ CDM model, in which the equation-of-state (EoS) parameter  $w$  of dark energy is assumed to be a constant. The Chevallier-Polarski-Linder (CPL) [18, 19] model of dark energy is a further extension to the  $\Lambda$ CDM model, in which the form of  $w(a) = w_0 + w_a(1 - a)$  with two free parameters  $w_0$  and  $w_a$  is proposed to describe the cosmological evolution of the EoS of dark energy. We will also consider the holographic dark energy (HDE) model in this work, which is a dynamical dark energy model based on the consideration of quantum effective field theory and holographic principle of quantum gravity [20, 21]. In the HDE model, the type (quintessence or quintom) and the cosmological evolution of dark energy are solely determined by a dimensionless constant  $c$  (note that this is not the speed of light). For more detailed studies on the HDE model, see e.g. Refs. [22–43]. In this work, we use these four typical, simple dark energy models, namely, the  $\Lambda$ CDM,  $w$ CDM, CPL, and HDE models, as examples to make an analysis for the real-time cosmology.

The structure of this paper is arranged as follows. In Sect. II, we present the analysis method and the observational data used in this work. In Sect. III, we report the constraint results of cosmological parameters and make some relevant discussions. In Sect. IV, the conclusion of this work is given.

## II. METHOD AND DATA

We will simulate the redshift drift data of SKA, and use these mock data to constrain the cosmological models. We will also simulate the redshift drift data of E-ELT, and to make comparison and combination with the data of SKA. In order to check how the redshift drift data of SKA will break the parameter degeneracies generated by

other cosmological observations, we will also consider the current mainstream observations in this work.

### A. Current mainstream cosmological observations

**SN data:** We use the largest compilation of type Ia supernovae (SN) data in this work, which is named the Pantheon compilation [44]. The Pantheon compilation consists of 1048 SN data, which is composed of the subset of 279 SN data from the Pan-STARRS1 Medium Deep Survey in the redshift range of  $0.03 < z < 0.65$  and useful distance estimates of SN from SDSS, SNLS, various low-redshift and HST samples in the redshift range of  $0.01 < z < 2.3$ . According to the observational point of view, using a modified version of the Tripp formula [45], in the SALT2 spectral model [46], the distance modulus can be expressed as [44]

$$\mu = m_B - M + \alpha \times x_1 - \beta \times c + \Delta_M + \Delta_B, \quad (1)$$

where  $m_B$ ,  $x_1$ , and  $c$  represent the log of the overall flux normalization, the light-curve shape parameter, and the color in the light-curve fit of SN, respectively,  $M$  represents the absolute B-band magnitude with  $x_1 = 0$  and  $c = 0$  for a fiducial SN,  $\alpha$  and  $\beta$  are the coefficients of the relation between luminosity and stretch and of the relation between luminosity and color, respectively,  $\Delta_M$  is the distance correction from the host-galaxy mass of the SN, and  $\Delta_B$  is the distance correction from predicted biases of simulations.

The luminosity distance  $d_L$  to a supernova can be given by

$$d_L(z) = \frac{1+z}{H_0} \int_0^z \frac{dz'}{E(z')}, \quad (2)$$

where  $E(z) \equiv H(z)/H_0$ . Note that we consider a flat universe throughout this work. The  $\chi^2$  function for SN observation is expressed as

$$\chi_{\text{SN}}^2 = (\mu - \mu_{\text{th}})^\dagger C_{\text{SN}}^{-1} (\mu - \mu_{\text{th}}), \quad (3)$$

where  $C_{\text{SN}}$  is the covariance matrix of the SN observation [44], and the theoretical distance modulus  $\mu_{\text{th}}$  is given by

$$\mu_{\text{th}} = 5 \log_{10} \frac{d_L}{10 \text{pc}}. \quad (4)$$

**CMB data:** For the cosmic microwave background (CMB) anisotropies data, we use the ‘‘Planck distance priors’’ from the Planck 2015 data [47]. The distance priors include the shift parameter  $R$ , the ‘‘acoustic scale’’  $\ell_A$ , and the baryon density  $\omega_b$ , defined by

$$R \equiv \sqrt{\Omega_m H_0^2 (1 + z_*)} D_A(z_*), \quad (5)$$

$$\ell_A \equiv (1 + z_*) \frac{\pi D_A(z_*)}{r_s(z_*)}, \quad (6)$$

$$\omega_b \equiv \Omega_b h^2, \quad (7)$$

where  $\Omega_m$  is the present-day fractional matter density, and  $D_A(z_*)$  denotes the angular diameter distance at  $z_*$  with  $z_*$  being the redshift of the decoupling epoch of photons. In a flat universe,  $D_A$  can be expressed as

$$D_A(z) = \frac{1}{H_0(1+z)} \int_0^z \frac{dz'}{E(z')}, \quad (8)$$

and  $r_s(a)$  can be given by

$$r_s(a) = \frac{1}{\sqrt{3}} \int_0^a \frac{da'}{a' H(a') \sqrt{1 + (3\Omega_b/4\Omega_\gamma)a'}}, \quad (9)$$

where  $\Omega_b$  and  $\Omega_\gamma$  are the present-day energy densities of baryons and photons, respectively. In this work, we adopt  $3\Omega_b/4\Omega_\gamma = 31500\Omega_b h^2 (T_{\text{cmb}}/2.7\text{K})^{-4}$  and  $T_{\text{cmb}} = 2.7255\text{K}$ .  $z_*$  can be calculated by the fitting formula [48],

$$z_* = 1048[1 + 0.00124(\Omega_b h^2)^{-0.738}][1 + g_1(\Omega_m h^2)^{g_2}], \quad (10)$$

where

$$g_1 = \frac{0.0783(\Omega_b h^2)^{-0.238}}{1 + 39.5(\Omega_b h^2)^{-0.76}}, \quad g_2 = \frac{0.560}{1 + 21.1(\Omega_b h^2)^{1.81}}. \quad (11)$$

The three values can be obtained from the Planck TT+LowP data [47]:  $R = 1.7488 \pm 0.0074$ ,  $\ell_A = 301.76 \pm 0.14$ , and  $\Omega_b h^2 = 0.02228 \pm 0.00023$ . The  $\chi^2$  function for CMB is

$$\chi_{\text{CMB}}^2 = \Delta p_i [\text{Cov}_{\text{CMB}}^{-1}(p_i, p_j)] \Delta p_j, \quad \Delta p_i = p_i^{\text{th}} - p_i^{\text{obs}}, \quad (12)$$

where  $p_1 = \ell_A$ ,  $p_2 = R$ ,  $p_3 = \omega_b$ , and  $\text{Cov}_{\text{CMB}}^{-1}$  is the inverse covariance matrix and can be found in Ref. [47].

**BAO data:** From the baryon acoustic oscillations (BAO) measurements, we can obtain the distance ratio  $D_V(z)/r_s(z_d)$  or  $D_M(z)/r_s(z_d)$ . The spherical average gives the expression of  $D_V(z)$ ,

$$D_V(z) \equiv \left[ D_M^2(z) \frac{z}{H(z)} \right]^{1/3}, \quad (13)$$

where  $D_M(z) = (1+z)D_A(z)$  is the the comoving angular diameter distance [49].  $r_s(z_d)$  is the comoving sound horizon size at the redshift  $z_d$  of the drag epoch and its calculated value can be given by Eq. (9).  $z_d$  is given by the fitting formula [48],

$$z_d = \frac{1291(\Omega_m h^2)^{0.251}}{1 + 0.659(\Omega_m h^2)^{0.828}} [1 + b_1(\Omega_b h^2)^{b_2}], \quad (14)$$

and

$$b_1 = 0.313(\Omega_m h^2)^{-0.419} [1 + 0.607(\Omega_m h^2)^{0.674}], \quad (15)$$

$$b_2 = 0.238(\Omega_m h^2)^{0.223}.$$

We use five BAO data points from the 6dF Galaxy Survey at  $z_{\text{eff}} = 0.106$  [50], the SDSS-DR7 at  $z_{\text{eff}} = 0.15$

[51], and the BOSS-DR12 at  $z_{\text{eff}} = 0.38$ ,  $z_{\text{eff}} = 0.51$ , and at  $z_{\text{eff}} = 0.61$  [49]. The distance ratio  $D_V(z)/r_s(z_d)$  or  $D_M(z)/r_s(z_d)$  for the BAO data are shown in Table I.

The  $\chi^2$  function for BAO measurements is

$$\chi_{\text{BAO}}^2 = \sum_{i=1}^5 \frac{(\xi_i^{\text{obs}} - \xi_i^{\text{th}})^2}{\sigma_i^2}, \quad (16)$$

where  $\xi_{\text{th}}$  and  $\xi_{\text{obs}}$  represent the theoretically predicted value and the experimentally measured value of the  $i$ -th data point for the BAO observations, respectively, and  $\sigma_i$  is the standard deviation of the  $i$ -th data point.

## B. Redshift drift observations from E-ELT and SKA

The actual measurement for the SL-test signal is the shift in the spectroscopic velocity ( $\Delta v$ ) for a source in a given time interval ( $\Delta t_o$ ). The spectroscopic velocity shift is usually expressed as [2]

$$\Delta v = \frac{\Delta z}{1+z} = H_0 \Delta t_o \left[ 1 - \frac{E(z)}{1+z} \right], \quad (17)$$

where  $E(z)$  is determined by a specific cosmological model.

The measurement of velocity shift will be achieved by the upcoming experiments such as the E-ELT and SKA through two different means. The E-ELT will be able to observe the Lyman- $\alpha$  absorption lines of distant quasar systems to achieve the measurement of  $\Delta v$  in the redshift range of  $z \in [2, 5]$  [2, 52]. The SKA will measure the spectroscopic velocity shift  $\Delta v$  by observing the neutral hydrogen emission signals of galaxies at the precision of one percent in the redshift range of  $z \in [0, 1]$ . Obviously, the E-ELT and SKA experiments will be the ideal complements with each other, because of the explorations of different periods for the cosmic evolution.

**E-ELT mock data:** For the E-ELT data, as discussed in Ref. [53], the standard deviation on  $\Delta v$  can be estimated as

$$\sigma_{\Delta v} = 1.35 \left( \frac{2370}{S/N} \right) \left( \frac{N_{\text{QSO}}}{30} \right)^{-1/2} \left( \frac{1 + z_{\text{QSO}}}{5} \right)^x \text{ cm s}^{-1}, \quad (18)$$

where  $S/N$  is the signal-to-noise ratio of the Lyman- $\alpha$  spectrum,  $N_{\text{QSO}}$  is the number of observed quasars at the effective redshift  $z_{\text{QSO}}$ , and  $x$  is 1.7 for  $2 \leq z \leq 4$  and 0.9 for  $z \geq 4$ . In this work, we assume  $S/N = 3000$  and  $N_{\text{QSO}} = 30$ . We generate 30 mock data with a uniform distribution for the E-ELT's redshift drift observation in six redshift bins (the redshift interval  $\Delta z = 0.5$  for each bin), and we assume the observation time of  $\Delta t_o = 10$  years.

**SKA mock data:** For the case of SKA, we follow the prescription given in Refs. [54, 55] to produce the mock data of redshift drift. It is shown in Refs. [54, 55] that if

TABLE I: Values of the distance ratio  $\xi(z) = D_V(z)/r_s(z_d)$  or  $D_M(z)/r_s(z_d)$  from the BAO measurements. Note that for each  $D_M(z)/r_s(z_d)$ , the first error is the statistical uncertainty, while the second value is the systematic error.

$z$	$\xi(z)$	Experiment	Reference
0.106	$D_V(z)/r_s(z_d) = 2.976 \pm 0.133$	6dFGS	[50]
0.15	$D_V(z)/r_s(z_d) = 4.466 \pm 0.168$	SDSS-DR7	[51]
0.38	$D_M(z)/r_s(z_d) = 10.231 \pm 0.149 \pm 0.074$	BOSS-DR12	[49]
0.51	$D_M(z)/r_s(z_d) = 13.364 \pm 0.183 \pm 0.095$	BOSS-DR12	[49]
0.61	$D_M(z)/r_s(z_d) = 15.611 \pm 0.223 \pm 0.115$	BOSS-DR12	[49]

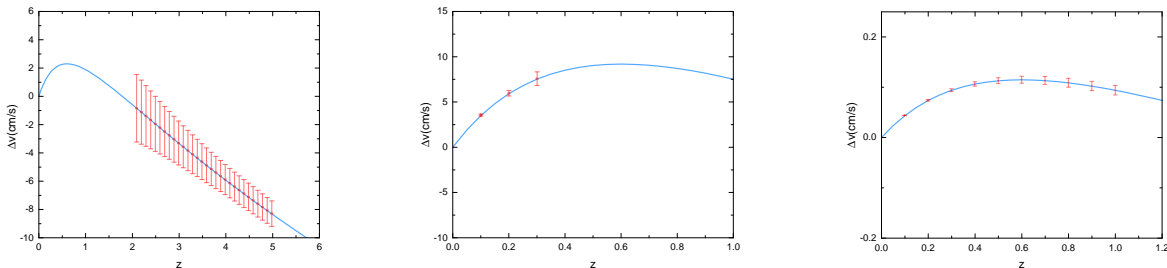


FIG. 1: Reconstructed redshift drift using the SN+CMB+BAO in the  $\Lambda$ CDM. The error bars on the curves are estimated from E-ELT (left panel), SKA1 (central panel) and SKA2 (right panel).

SKA could have the full sensitivity and detect a billion galaxies, the evolution of the frequency shift in redshift space would be estimated to a precision of one percent. Thus we consider the following two scenarios:

1. For SKA Phase 1, in our simulation, we produce 3 mock data of the drift  $\Delta v$  in redshift bin centered on  $z_i = [0.1, 0.2, 0.3]$  with velocity uncertainties  $\sigma_{\Delta v}$  respectively of 3% in the first bin, 5% in the second bin and 10% in the third bin. The redshift interval  $\Delta z$  is 0.1 for each bin and the timespan  $\Delta t_o$  is 40 years. Note that although a timespan of 40 years is long integration time, it can be as a benchmark scenario to improve sensitivity and redshift coverage in the full SKA configuration.
2. For SKA Phase 2, we generate 10 mock data of the drift  $\Delta v$  in ten redshift bins. The mock data are covering from  $z = 0.1$  to  $z = 1.0$  with the velocity uncertainties  $\sigma_{\Delta v}$  ranging from 1% to 10%. This could be reached in the timespan  $\Delta t_o = 0.5$  years, which leads to an extremely competitive and ideal scenario. Note that the requirement of this scenario is  $10^7$  galaxies observed in each bin [55].

In addition, in the mock data simulation, we adopt the scheme accordant with our previous papers [3–6, 56, 57]. In other words, the fiducial cosmology for the SL simulated data from the E-ELT or the SKA is chosen to be the best fit result of the analysis of the data com-

bination of SN+CMB+BAO in the  $\Lambda$ CDM model, the  $w$ CDM model, the CPL model, and the HDE model.

### III. RESULTS AND DISCUSSION

Since the  $\Lambda$ CDM model is widely regarded as a prototype of the standard cosmology, we take this model as a reference model to test the constraining power of the SKA-only mock data and make an analysis of constraints on cosmological parameters when the redshift drift data of SKA and E-ELT are combined. In Fig. 1, the mock  $\Delta v$  data and their errors in the  $\Lambda$ CDM model are presented. We find that in the E-ELT the error of  $\Delta v$  decreases with the increase of redshift, and vice versa in the SKA1 or SKA2. In Fig. 2, we plot the two-dimensional posterior contours at 68% and 95% confidence level (CL) in the  $\Lambda$ CDM model. We clearly see that using the SKA1-only mock data, the  $\Lambda$ CDM model can only be loosely constrained, while the model can be well constrained using the SKA2-only mock data.

In addition, from Fig. 2, we clearly see that in the  $\Lambda$ CDM model, from the E-ELT,  $\Omega_m$  and  $h$  are in strong anti-correlation while constraints from SKA1 or SKA2 provide a positive correlation for  $\Omega_m$  and  $h$ , and thus the orthogonality of the two degeneracy orientations leads to a complete breaking for the parameter degeneracy. Thus, the constraints from the combination of E-ELT and SKA (SKA1 or SKA2) would have a tremendous im-

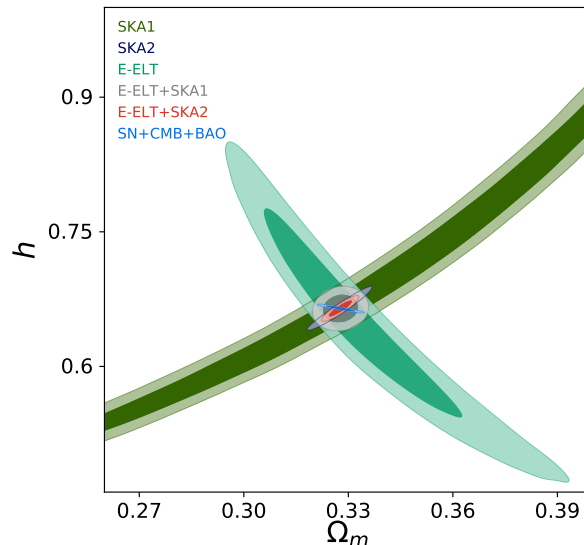


FIG. 2: Constraints ( $1\sigma$  and  $2\sigma$  CL) on the  $\Lambda$ CDM in the  $\Omega_m$ - $h$  plane by using the SKA1, SKA2, E-ELT, E-ELT+SKA1, E-ELT+SKA2, and SN+CMB+BAO data.

provement, as shown by the gray and red contours in Fig. 2. Particularly, the results from the combination of E-ELT+SKA2 are almost as good as the constraint from the combination of SN+CMB+BAO, which implies that the redshift drift observation would have chance to be one of the most competitive cosmological probes.

Meanwhile, we find that the degeneracy orientation of E-ELT+SKA1 or E-ELT+SKA2 in the parameter plane is evidently different from the combination of SN+CMB+BAO. This phenomenon would result in an effective breaking of the parameter degeneracy and a significant improvement of the constraints on dark energy. It is of extreme interest to know what role the redshift drift data of SKA will play in constraining dark energy in the future. Next we will explore this issue in detail.

We constrain the  $\Lambda$ CDM,  $w$ CDM, CPL and HDE models by using the data combinations of SN+CMB+BAO, SN+CMB+BAO+E-ELT, SN+CMB+BAO+E-ELT+SKA1, and SN+CMB+BAO+E-ELT+SKA2 to complete our analysis. The constraint results are presented in Tables II-IV and Figs. 3-4. In Table II, we show the best-fit results with the  $1\sigma$  errors quoted. The constraint errors and precisions of the cosmological parameters are given in Tables III-IV, respectively. Here, the error is taken to be the root-mean-square, i.e.,  $\sigma = [(\sigma_+^2 + \sigma_-^2)/2]^{1/2}$ , and the precision for a parameter  $\xi$  is defined as  $\xi = \sigma/\xi_{bf}$ , where  $\xi_{bf}$  represents the best-fit value for a parameter  $\xi$ . In Figs. 3-4, we show the two-dimensional posterior distribution contours of constraint results in the  $\Lambda$ CDM,  $w$ CDM, CPL and HDE models at the 68% and 95% CL.

From these figures, we clearly see that when the E-ELT mock data are combined with SN+CMB+BAO, the parameter spaces can be significantly reduced in the  $\Lambda$ CDM,  $w$ CDM, and HDE models, while there is

little significant improvement in the parameter space for the CPL model. Adding the SKA1 mock data to the data combination of SN+CMB+BAO+E-ELT, the parameter spaces are sharply reduced. In particular, when the SKA2 mock data are combined with SN+CMB+BAO+E-ELT, the improvement is even more significant than the case of SN+CMB+BAO+E-ELT+SKA1. Meanwhile, from Fig. 4, we can easily find that the E-ELT and SKA mock data can help to break the parameter degeneracies, in particular between the parameters  $\Omega_m$  and  $c$  in the HDE model.

From Table IV, we can easily find that the E-ELT, SKA1, and SKA2 can significantly improve the constraints on almost all the parameters in different extent, in particular for SKA2. Concretely, when the E-ELT mock data are combined with SN+CMB+BAO, the precision of  $\Omega_m$  is improved from 1.19% to 1.07% in the  $\Lambda$ CDM model, from 1.60% to 1.35% in the  $w$ CDM model, from 1.72% to 1.30% in the HDE model. The precision of  $h$ ,  $w$ , and  $c$  are also enhanced in the  $\Lambda$ CDM,  $w$ CDM, and HDE models; for details, see Table IV. Adding the SKA1 mock data to the data combination of SN+CMB+BAO+E-ELT, the improvement of the parameter  $\Omega_m$  is from 1.07% to 0.88% in the  $\Lambda$ CDM model, from 1.35% to 1.20% in the  $w$ CDM model, from 1.66% to 1.25% in the CPL model, and from 1.30% to 0.97% in the HDE model. For the parameter  $h$ , the constraint is improved from 0.39% to 0.35% in the  $\Lambda$ CDM model, from 0.97% to 0.75% in the  $w$ CDM model, from 0.94% to 0.76% in the CPL model, and from 0.86% to 0.37%. For property of dark energy, the improvement is from 4.38% to 3.98% for the parameter  $w$  in the  $w$ CDM model, from 5.55% to 4.68% for the parameter  $w_0$  in the CPL model, from 34.46% to 31.62% for the parameter  $w_a$  in the CPL model, and from 5.49% to 2.05% for the parameter  $c$  in

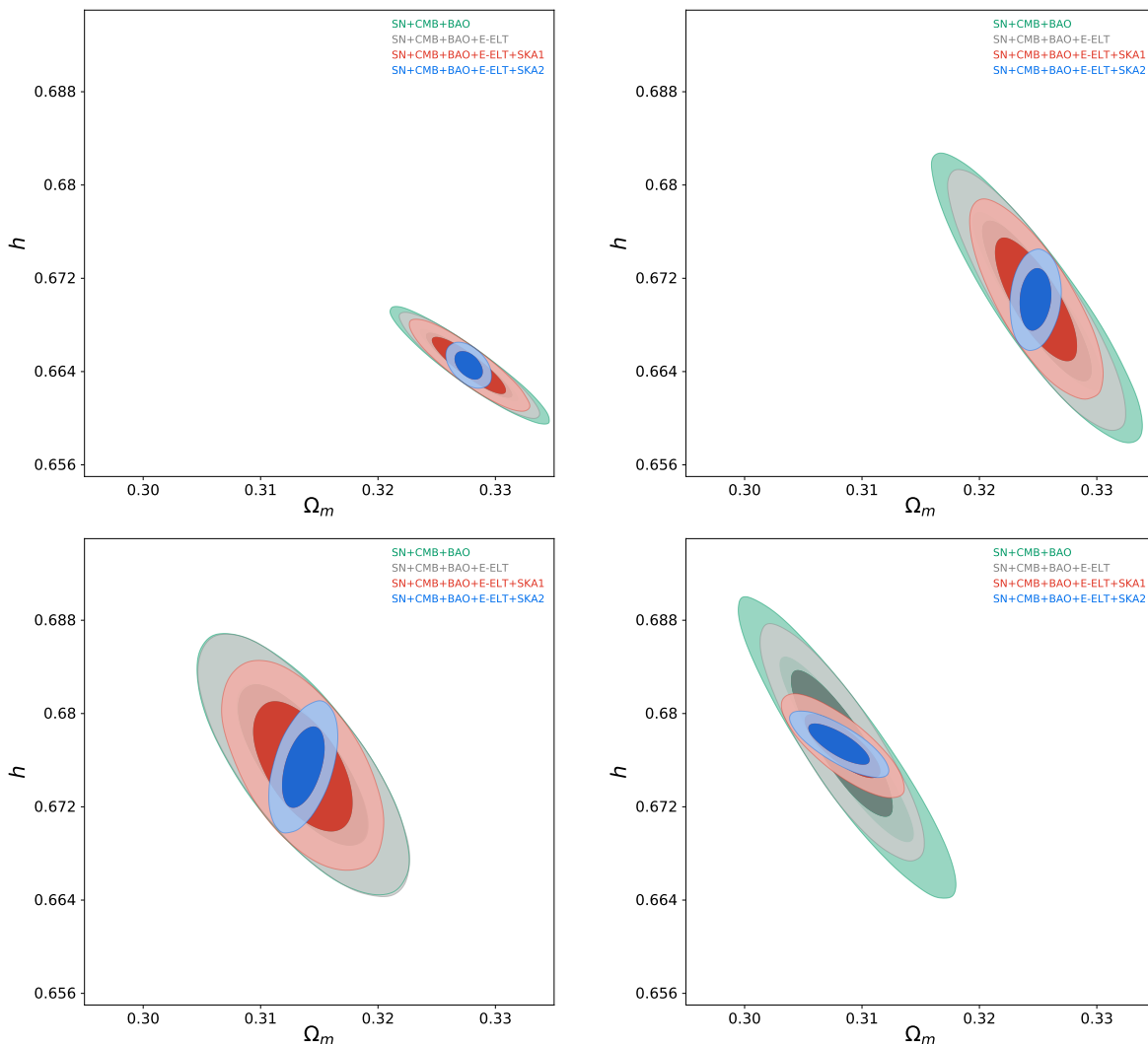


FIG. 3: Constraints ( $1\sigma$  and  $2\sigma$  CL) on the  $\Lambda$ CDM,  $w$ CDM, CPL, and HDE models from the SN+CMB+BAO, SN+CMB+BAO+E-ELT, SN+CMB+BAO+E-ELT+SKA1, and SN+CMB+BAO+E-ELT+SKA2 data in the  $\Omega_m$ - $h$  plane.

the HDE model.

Furthermore, when the SKA2 mock data are combined with SN+CMB+BAO+E-ELT, the improvement of the parameter  $\Omega_m$  is from 1.07% to 0.34% in the  $\Lambda$ CDM model, from 1.35% to 0.40% in the  $w$ CDM model, from 1.66% to 0.54% in the CPL model, and from 1.30% to 0.81% in the HDE model. For the parameter  $h$ , the constraint is improved from 0.39% to 0.18% in the  $\Lambda$ CDM model, from 0.97% to 0.37% in the  $w$ CDM model, from 0.94% to 0.47% in the CPL model, and from 0.86% to 0.25% in the HDE model. For property of dark energy, the improvement is from 4.38% to 2.99% for the parameter  $w$  in the  $w$ CDM model, from 5.55% to 3.57% for the parameter  $w_0$  in the CPL model, from 34.46% to 29.06% for the parameter  $w_a$  in the CPL model, and from 5.49% to 1.16% for the parameter  $c$  in the HDE model. Therefore, we conclude that the redshift drift data of SKA will help to significantly improve the constraints and break

the degeneracy between the parameters in constraining dark energy in the future.

#### IV. CONCLUSION

In this work, we wish to investigate what extent the cosmological parameters can be constrained to when the redshift drift data of SKA are used and what will happen when the combination of SKA and E-ELT mock data are considered. We use the five data sets, i.e., SKA1, SKA2, E-ELT, E-ELT+SKA1, E-ELT+SKA2, and SN+CMB+BAO to reach our aims in the  $\Lambda$ CDM model. We find that using the SKA2 mock data alone, the  $\Lambda$ CDM model can be constrain well, while the constraint is weak from the mock data of SKA1-only. When the redshift drift mock data of SKA and E-ELT are combined, the results show that the parameter space is dra-

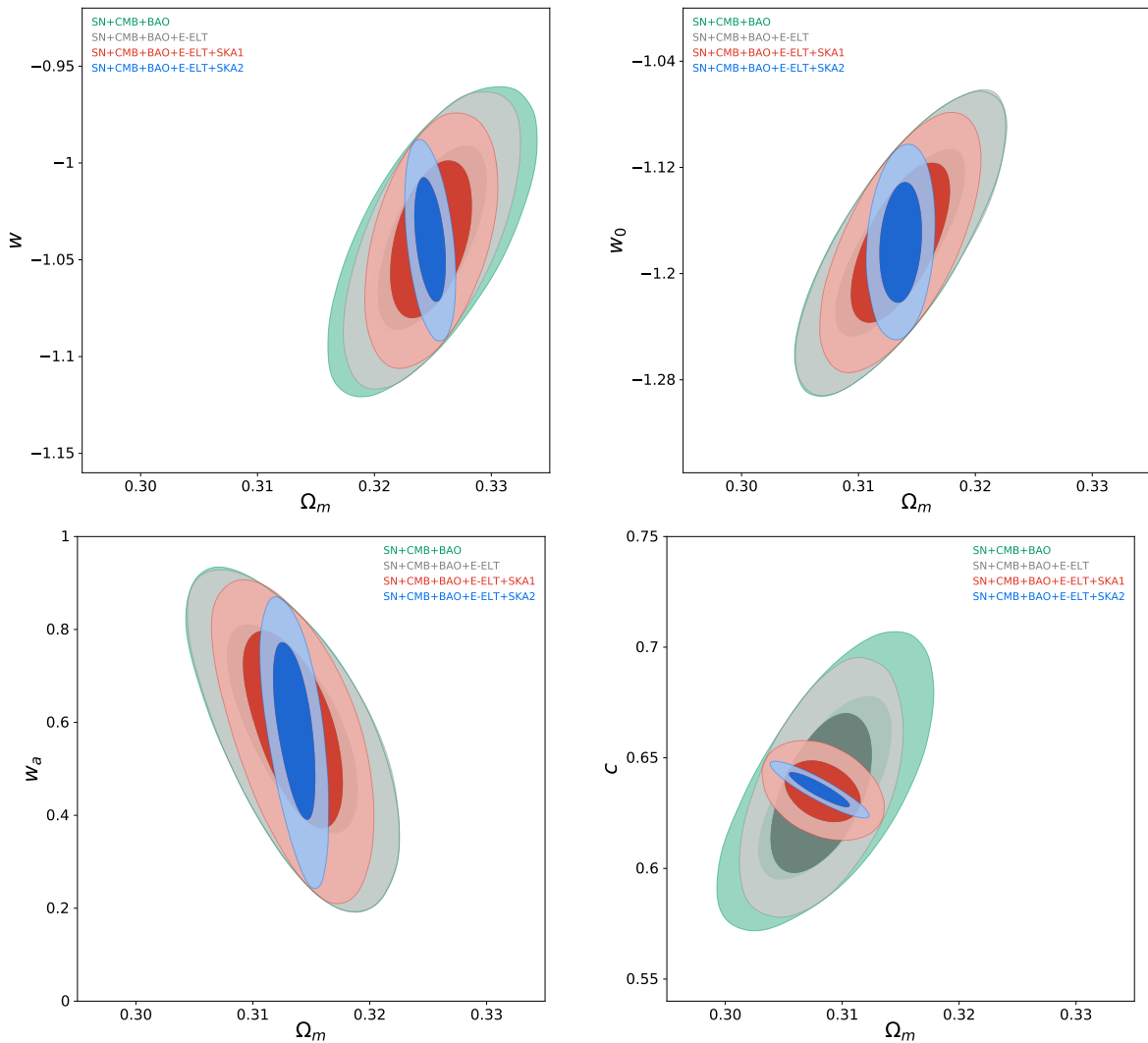


FIG. 4: Constraints ( $1\sigma$  and  $2\sigma$  CL) in the  $\Omega_m$ - $w$  plane for  $w$ CDM model, in the  $\Omega_m$ - $w_0$  plane for CPL model, in the  $\Omega_m$ - $w_a$  plane for CPL model, and in the  $\Omega_m$ - $c$  plane for HDE model from the SN+CMB+BAO, SN+CMB+BAO+E-ELT, SN+CMB+BAO+E-ELT+SKA1, and SN+CMB+BAO+E-ELT+SKA2 data.

matically reduced almost as good as SN+CMB+BAO. Thus, the last aim of this work is to investigate what role the redshift drift data of SKA will play in constraining dark energy in the future. To fulfill the task, we employ several concrete dark energy models, including the  $\Lambda$ CDM,  $w$ CDM, CPL, and HDE models, which are still consistent with the current observations at least to some extent.

We first use the data combination of SN+CMB+BAO to constrain the four dark energy models, and then we consider the addition of the E-ELT mock data in the data combination, i.e., we use the data combination of SN+CMB+BAO+E-ELT to constrain the models. The constraints on cosmological parameters are tremendously improved for the  $\Lambda$ CDM,  $w$ CDM, and HDE models, while E-ELT mock data do not help improve constraints in the CPL model. When adding the SKA1 mock data to

the SN+CMB+BAO+E-ELT, the constraint results are significantly improved in all the four dark energy models. For example, with the help of the SKA1 mock data, the constraints on  $\Omega_m$  are improved by 10%–25%, and the constraints on  $h$  are improved by 10%–70%. Furthermore, when the SKA2 mock data are combine with the dataset of SN+CMB+BAO+E-ELT, the constraint results are tremendously promoted in all the four dark energy models. Concretely, the constraints on  $\Omega_m$  are promoted by 40%–70%, and the constraints on  $h$  are promoted by 50%–75%. We also find that the degeneracy between cosmological parameters could be effectively broken by the combination of the E-ELT and SKA mock data. Therefore, we can conclude that in the future the redshift-drift observation of SKA would help to improve the constraints in constraining dark energy and have a good potential to be one of the most competitive cosmo-

TABLE II: Fitting results of parameters in the  $\Lambda$ CDM,  $w$ CDM, CPL, and HDE models using SN+CMB+BAO, SN+CMB+BAO+E-ELT, SN+CMB+BAO+E-ELT+SKA1, and SN+CMB+BAO+E-ELT+SKA2.

Parameter	SN+CMB+BAO				SN+CMB+BAO+E-ELT			
	$\Lambda$ CDM	$w$ CDM	CPL	HDE	$\Lambda$ CDM	$w$ CDM	CPL	HDE
$w_0$	—	$-1.0401^{+0.0477}_{-0.0452}$	$-1.1777^{+0.0614}_{-0.0683}$	—	—	$-1.0385^{+0.0442}_{-0.0447}$	$-1.1792^{+0.0644}_{-0.0663}$	—
$w_a$	—	—	$0.6028^{+0.1989}_{-0.2096}$	—	—	—	$0.6012^{+0.2036}_{-0.2107}$	—
$c$	—	—	—	$0.6350^{+0.0391}_{-0.0374}$	—	—	—	$0.6318^{+0.0358}_{-0.0316}$
$\Omega_m$	$0.3277^{+0.0039}_{-0.0039}$	$0.3248^{+0.0054}_{-0.0049}$	$0.3135^{+0.0050}_{-0.0053}$	$0.3086^{+0.0052}_{-0.0054}$	$0.3277^{+0.0035}_{-0.0034}$	$0.3250^{+0.0043}_{-0.0044}$	$0.3136^{+0.0049}_{-0.0055}$	$0.3082^{+0.0039}_{-0.0041}$
$h$	$0.6645^{+0.0029}_{-0.0029}$	$0.6702^{+0.0069}_{-0.0074}$	$0.6751^{+0.0067}_{-0.0060}$	$0.6770^{+0.0077}_{-0.0072}$	$0.6646^{+0.0026}_{-0.0026}$	$0.6700^{+0.0065}_{-0.0065}$	$0.6751^{+0.0065}_{-0.0062}$	$0.6776^{+0.0058}_{-0.0058}$
Parameter	SN+CMB+BAO+E-ELT+SKA1				SN+CMB+BAO+E-ELT+SKA2			
	$\Lambda$ CDM	$w$ CDM	CPL	HDE	$\Lambda$ CDM	$w$ CDM	CPL	HDE
$w_0$	—	$-1.0382^{+0.0373}_{-0.0392}$	$-1.1805^{+0.0565}_{-0.0541}$	—	—	$-1.0383^{+0.0288}_{-0.0310}$	$-1.1764^{+0.0395}_{-0.0443}$	—
$w_a$	—	—	$0.6103^{+0.1753}_{-0.2093}$	—	—	—	$0.0616^{+0.1615}_{-0.1871}$	—
$c$	—	—	—	$0.6345^{+0.0134}_{-0.0125}$	—	—	—	$0.6354^{+0.0075}_{-0.0072}$
$\Omega_m$	$0.3277^{+0.0029}_{-0.0029}$	$0.3248^{+0.0032}_{-0.0033}$	$0.3132^{+0.0040}_{-0.0037}$	$0.3082^{+0.0032}_{-0.0028}$	$0.3277^{+0.0011}_{-0.0011}$	$0.3248^{+0.0013}_{-0.0012}$	$0.3135^{+0.0017}_{-0.0016}$	$0.3081^{+0.0024}_{-0.0025}$
$h$	$0.6645^{+0.0023}_{-0.0023}$	$0.6701^{+0.0050}_{-0.0049}$	$0.6753^{+0.0050}_{-0.0052}$	$0.6773^{+0.0024}_{-0.0026}$	$0.6645^{+0.0011}_{-0.0013}$	$0.6701^{+0.0026}_{-0.0024}$	$0.6750^{+0.0034}_{-0.0030}$	$0.6774^{+0.0017}_{-0.0016}$

TABLE III: Constraint errors of parameters in the  $\Lambda$ CDM,  $w$ CDM, CPL, and HDE models using SN+CMB+BAO, SN+CMB+BAO+E-ELT, SN+CMB+BAO+E-ELT+SKA1, and SN+CMB+BAO+E-ELT+SKA2.

Error	SN+CMB+BAO				SN+CMB+BAO+E-ELT			
	$\Lambda$ CDM	$w$ CDM	CPL	HDE	$\Lambda$ CDM	$w$ CDM	CPL	HDE
$w_0$	—	0.0465	0.0649	—	—	0.0445	0.0654	—
$w_a$	—	—	0.2041	—	—	—	0.2071	—
$c$	—	—	—	0.0383	—	—	—	0.0338
$\Omega_m$	0.0039	0.0052	0.0052	0.0053	0.0035	0.0044	0.0052	0.0040
$h$	0.0029	0.0072	0.0064	0.0075	0.0026	0.0065	0.0064	0.0058
Error	SN+CMB+BAO+E-ELT+SKA1				SN+CMB+BAO+E-ELT+SKA2			
	$\Lambda$ CDM	$w$ CDM	CPL	HDE	$\Lambda$ CDM	$w$ CDM	CPL	HDE
$w_0$	—	0.0383	0.0553	—	—	0.0288	0.0357	—
$w_a$	—	—	0.1930	—	—	—	0.2906	—
$c$	—	—	—	0.0130	—	—	—	0.0116
$\Omega_m$	0.0029	0.0039	0.0039	0.0030	0.0011	0.0013	0.0054	0.0081
$h$	0.0023	0.0050	0.0051	0.0025	0.0018	0.0037	0.0047	0.0025

logical probes in constraining dark energy.

11835009, 11522540, and 11690021) and the Top-Notch Young Talents Program of China.

### Acknowledgments

This work was supported by the National Natural Science Foundation of China (Grant Nos. 11875102,

TABLE IV: Constraint precisions of parameters in the  $\Lambda$ CDM,  $w$ CDM, CPL, and HDE models using SN+CMB+BAO, SN+CMB+BAO+E-ELT, SN+CMB+BAO+E-ELT+SKA1, and SN+CMB+BAO+E-ELT+SKA2.

Precision	SN+CMB+BAO				SN+CMB+BAO+E-ELT			
	$\Lambda$ CDM	$w$ CDM	CPL	HDE	$\Lambda$ CDM	$w$ CDM	CPL	HDE
$w_0$	—	0.0447	0.0551	—	—	0.0438	0.0555	—
$w_a$	—	—	0.3386	—	—	—	0.3446	—
$c$	—	—	—	0.0603	—	—	—	0.0549
$\Omega_m$	0.0119	0.0160	0.0166	0.0172	0.0107	0.0135	0.0166	0.0130
$h$	0.0044	0.0107	0.0095	0.0111	0.0039	0.0097	0.0094	0.0086
Precision	SN+CMB+BAO+E-ELT+SKA1				SN+CMB+BAO+E-ELT+SKA2			
	$\Lambda$ CDM	$w$ CDM	CPL	HDE	$\Lambda$ CDM	$w$ CDM	CPL	HDE
$w_0$	—	0.0398	0.0468	—	—	0.0299	0.0357	—
$w_a$	—	—	0.3162	—	—	—	0.2906	—
$c$	—	—	—	0.0205	—	—	—	0.0116
$\Omega_m$	0.0088	0.0120	0.0125	0.0097	0.0034	0.0040	0.0054	0.0081
$h$	0.0035	0.0075	0.0076	0.0037	0.0018	0.0037	0.0047	0.0025

- [1] A. Sandage, *Astrophys. J.* **136**, 319 (1962).
- [2] A. Loeb, *Astrophys. J.* **499**, L111 (1998) [astro-ph/9802122].
- [3] J. J. Geng, J. F. Zhang and X. Zhang, *JCAP* **1407**, 006 (2014) [arXiv:1404.5407 [astro-ph.CO]].
- [4] J. J. Geng, J. F. Zhang and X. Zhang, *JCAP* **1412**, no. 12, 018 (2014) [arXiv:1407.7123 [astro-ph.CO]].
- [5] R. Y. Guo and X. Zhang, *Eur. Phys. J. C* **76**, no. 3, 163 (2016) [arXiv:1512.07703 [astro-ph.CO]].
- [6] D. Z. He, J. F. Zhang and X. Zhang, *Sci. China Phys. Mech. Astron.* **60** (2017) no.3, 039511 doi:10.1007/s11433-016-0472-1 [arXiv:1607.05643 [astro-ph.CO]].
- [7] Y. Liu, R. Y. Guo, J. F. Zhang and X. Zhang, *JCAP* **1905**, 016 (2019) [arXiv:1811.12131 [astro-ph.CO]].
- [8] R. Lazkoz, I. Leanizbarrutia and V. Salzano, *Eur. Phys. J. C* **78**, no. 1, 11 (2018) [arXiv:1712.07555 [astro-ph.CO]].
- [9] M. J. Zhang and W. B. Liu, arXiv:1311.6858 [astro-ph.CO].
- [10] M. Martinelli *et al.*, *Phys. Rev. D* **86**, 123001 (2012) [arXiv:1210.7166 [astro-ph.CO]].
- [11] P. S. Corasaniti, D. Huterer and A. Melchiorri, *Phys. Rev. D* **75**, 062001 (2007) [astro-ph/0701433].
- [12] A. Balbi and C. Quercellini, *Mon. Not. R. Astron. Soc.* **382**, 1623 (2007) [arXiv:0704.2350 [astro-ph]].
- [13] H. B. Zhang, W. H. Zhong, Z. H. Zhu and S. He, *Phys. Rev. D* **76**, 123508 (2007) [arXiv:0705.4409 [astro-ph]].
- [14] I. Zlatev, L. M. Wang and P. J. Steinhardt, *Phys. Rev. Lett.* **82**, 896 (1999) [astro-ph/9807002].
- [15] P. J. Steinhardt, L. M. Wang and I. Zlatev, *Phys. Rev. D* **59**, 123504 (1999) [astro-ph/9812313].
- [16] S. Mendoza and J. C. Hidalgo, *eConf C* **041213**, 2217 (2004) [astro-ph/0503307].
- [17] X. Zhang, *Phys. Lett. B* **611**, 1 (2005) [astro-ph/0503075].
- [18] M. Chevallier and D. Polarski, *Int. J. Mod. Phys. D* **10**, 213 (2001) [gr-qc/0009008].
- [19] E. V. Linder, *Phys. Rev. Lett.* **90**, 091301 (2003) [astro-ph/0208512].
- [20] M. Li, X. D. Li, S. Wang and X. Zhang, *JCAP* **0906**, 036 (2009) [arXiv:0904.0928 [astro-ph.CO]].
- [21] M. Li, X. Li and X. Zhang, *Sci. China Phys. Mech. Astron.* **53**, 1631 (2010) [arXiv:0912.3988 [astro-ph.CO]].
- [22] M. Li, *Phys. Lett. B* **603**, 1 (2004) [hep-th/0403127].
- [23] X. Zhang and F. Q. Wu, *Phys. Rev. D* **72**, 043524 (2005) [astro-ph/0506310].
- [24] X. Zhang and F. Q. Wu, *Phys. Rev. D* **76**, 023502 (2007) [astro-ph/0701405].
- [25] X. Zhang, *Phys. Lett. B* **648**, 1 (2007) doi:10.1016/j.physletb.2007.02.069 [astro-ph/0604484].
- [26] X. Zhang, *Phys. Rev. D* **74**, 103505 (2006) doi:10.1103/PhysRevD.74.103505 [astro-ph/0609699].
- [27] J. Zhang, X. Zhang and H. Liu, *Phys. Lett. B* **651**, 84 (2007) doi:10.1016/j.physletb.2007.06.019 [arXiv:0706.1185 [astro-ph]].
- [28] J. f. Zhang, X. Zhang and H. y. Liu, *Eur. Phys. J. C* **52**, 693 (2007) doi:10.1140/epjc/s10052-007-0408-2 [arXiv:0708.3121 [hep-th]].
- [29] J. F. Zhang, X. Zhang and H. Liu, *Eur. Phys. J. C* **54**, 303 (2008) doi:10.1140/epjc/s10052-008-0532-7 [arXiv:0801.2809 [astro-ph]].
- [30] C. Gao, F. Wu, X. Chen and Y. G. Shen, *Phys. Rev. D* **79**, 043511 (2009) [arXiv:0712.1394 [astro-ph]].
- [31] X. Zhang, *Phys. Rev. D* **79**, 103509 (2009) doi:10.1103/PhysRevD.79.103509 [arXiv:0901.2262]

- [astro-ph.CO]].
- [32] J. L. Cui, L. Zhang, J. F. Zhang and X. Zhang, *Chin. Phys. B* **19**, 019802 (2010) doi:10.1088/1674-1056/19/1/019802 [arXiv:0902.0716 [astro-ph.CO]].
- [33] C. J. Feng and X. Zhang, *Phys. Lett. B* **680**, 399 (2009) doi:10.1016/j.physletb.2009.09.040 [arXiv:0904.0045 [gr-qc]].
- [34] Y. H. Li, S. Wang, X. D. Li and X. Zhang, *JCAP* **1302**, 033 (2013) doi:10.1088/1475-7516/2013/02/033 [arXiv:1207.6679 [astro-ph.CO]].
- [35] J. F. Zhang, M. M. Zhao, J. L. Cui and X. Zhang, *Eur. Phys. J. C* **74**, no. 11, 3178 (2014) doi:10.1140/epjc/s10052-014-3178-7 [arXiv:1409.6078 [astro-ph.CO]].
- [36] J. L. Cui and J. F. Zhang, *Eur. Phys. J. C* **74**, 2849 (2014) [arXiv:1402.1829 [astro-ph.CO]].
- [37] J. F. Zhang, J. L. Cui and X. Zhang, *Eur. Phys. J. C* **74**, no. 10, 3100 (2014) [arXiv:1409.6562 [astro-ph.CO]].
- [38] J. F. Zhang, M. M. Zhao, Y. H. Li and X. Zhang, *JCAP* **1504**, 038 (2015) doi:10.1088/1475-7516/2015/04/038 [arXiv:1502.04028 [astro-ph.CO]].
- [39] X. Zhang, *Phys. Rev. D* **93**, no. 8, 083011 (2016) doi:10.1103/PhysRevD.93.083011 [arXiv:1511.02651 [astro-ph.CO]].
- [40] S. Wang, Y. F. Wang, D. M. Xia and X. Zhang, *Phys. Rev. D* **94**, no. 8, 083519 (2016) doi:10.1103/PhysRevD.94.083519 [arXiv:1608.00672 [astro-ph.CO]].
- [41] M. M. Zhao, D. Z. He, J. F. Zhang and X. Zhang, *Phys. Rev. D* **96**, no. 4, 043520 (2017) doi:10.1103/PhysRevD.96.043520 [arXiv:1703.08456 [astro-ph.CO]].
- [42] L. Feng, Y. H. Li, F. Yu, J. F. Zhang and X. Zhang, *Eur. Phys. J. C* **78**, no. 10, 865 (2018) doi:10.1140/epjc/s10052-018-6338-3 [arXiv:1807.03022 [astro-ph.CO]].
- [43] J. F. Zhang, H. Y. Dong, J. Z. Qi and X. Zhang, arXiv:1906.07504 [astro-ph.CO].
- [44] D. M. Scolnic *et al.*, *Astrophys. J.* **859**, no. 2, 101 (2018) [arXiv:1710.00845 [astro-ph.CO]].
- [45] R. Tripp, *A&A* **331**, 815 (1998)
- [46] SNLS Collaboration (J. Guy *et al.*) *A&A* **523** (2010) A7 [arXiv:1010.4743[astro-ph.CO]]
- [47] P. A. R. Ade *et al.* [Planck Collaboration], *Astron. Astrophys.* **594**, A14 (2016) [arXiv:1502.01590 [astro-ph.CO]].
- [48] W. Hu and N. Sugiyama, *Astrophys. J.* **471**, 542 (1996) [astro-ph/9510117].
- [49] S. Alam *et al.* [BOSS Collaboration], *Mon. Not. Roy. Astron. Soc.* **470**, no. 3, 2617 (2017) [arXiv:1607.03155 [astro-ph.CO]].
- [50] F. Beutler *et al.*, *Mon. Not. Roy. Astron. Soc.* **416**, 3017 (2011) [arXiv:1106.3366 [astro-ph.CO]].
- [51] A. J. Ross, L. Samushia, C. Howlett, W. J. Percival, A. Burden and M. Manera, *Mon. Not. Roy. Astron. Soc.* **449**, no. 1, 835 (2015) [arXiv:1409.3242 [astro-ph.CO]].
- [52] J. Liske *et al.*, Top Level Requirements For ELT-HIRES, Document ESO 204697 Version 1 (2014).
- [53] J. Liske *et al.*, *Mon. Not. Roy. Astron. Soc.* **386**, 1192 (2008) [arXiv:0802.1532 [astro-ph]].
- [54] H. R. Klckner *et al.*, *PoS AASKA* **14**, 027 (2015) [arXiv:1501.03822 [astro-ph.CO]].
- [55] C. J. A. P. Martins, M. Martinelli, E. Calabrese and M. P. L. P. Ramos, *Phys. Rev. D* **94**, no. 4, 043001 (2016) [arXiv:1606.07261 [astro-ph.CO]].
- [56] J. J. Geng, R. Y. Guo, A. Wang, J. F. Zhang and X. Zhang, *Commun. Theor. Phys.* **70**, no. 4, 445 (2018) [arXiv:1806.10735 [astro-ph.CO]].
- [57] J. J. Geng, Y. H. Li, J. F. Zhang and X. Zhang, *Eur. Phys. J. C* **75**, no. 8, 356 (2015) [arXiv:1501.03874 [astro-ph.CO]].